PHYSICAL REVIEW A VOLUME 8, NUMBER 3 SEPTEMBER 1973

# Numerical Experiments on the Stochastic Behavior of a Lennard-Jones Gas System*

Spotswood D. Stoddard and Joseph Ford
*School of Physics, Georgia Institute of Technology, Atlanta, Georgia 30332*

(Received 18 May 1973)

It is known that the hard-sphere gas exhibits strongly stochastic properties. For it, most initially close phase-space-trajectory pairs separate exponentially with time, and Sinai has used this so-called $C$-system behavior to develop a rigorous proof of ergodicity and mixing in the hard-sphere gas. In this paper we numerically integrate the equations of motion for a Lennard-Jones gas, which has attractive as well as repulsive interparticle forces, and we demonstrate that this exponential separation of initially close trajectory pairs persists even in the presence of attractive forces over a fairly wide range of particle densities. In our calculations, this range extends from the dilute-gas region up to densities at which three-body and four-body collisions become significant. Moreover for this density range, we show that an expression for the trajectory-pair rate of exponential separation, rather crudely derived for a hard-sphere gas, fits the empirical Lennard-Jones data quite nicely. Our evidence thus indicates that a gas system with attractive forces can exhibit $C$-system behavior similar to that of the hard-sphere gas. Finally we point out that the exponential separation of trajectories as empirically observed here involves an unusual type of correlated collision sequence.

## I. INTRODUCTION

Boltzmann and Gibbs, in an act of faith, founded[1] their theories of statistical mechanics on the assumption that the phase-space trajectories for isolated mechanical systems are extremely wild and erratic paths wandering freely over the energy surface and spending equal times in equal hyperareas of this surface. To an extent their faith has recently been justified by Sinai, who rigorously proves[2] that the hard-sphere gas is an unstable[3] system in the sense that almost every initially close trajectory pair separates exponentially with time. In particular Sinai proves[2,3] that this exponential instability is sufficient to guarantee ergodicity and mixing for the hard-sphere gas.

Although the extension of Sinai's results to systems having purely repulsive interparticle forces is expected[4] to be straightforward, mathematicians anticipate severe problems[4] in extending the proof to systems having attractive as well as repulsive interparticle forces. It is conjectured that the inclusion of attractive forces will cause a breakdown of ergodicity on at least some energy surfaces. In particular, if the system energy is sufficiently low or the system density sufficiently high, one anticipates finding energy surfaces which contain nonergodic subregions of Kolmogorov-Arnold-Moser (KAM) stability[5] embedded in perhaps an otherwise "ergodic sea"; indeed a number of empirical computer studies[6] support this conjecture. Despite all these conjectures, we here suggest that the anticipated difficulties may, in a sense, be largely mathematical rather than physical. For example, even were stable KAM regions to exist at all energies, nothing now known precludes their being so small as to be physically irrelevant—except perhaps for questions regarding metastability—while nonetheless remaining mathematically troublesome. Equally, nothing precludes the existence of a critical energy,[5] depending perhaps on various system parameters, above which systems with attractive forces are no less ergodic than the hard-sphere gas. In order to provide empirical support for these latter possibilities, we have conducted the numerical experiments described herein.

In this paper, we consider a Lennard-Jones gas which has an attractive as well as a repulsive term in the interparticle potential, and we demonstrate that this gas system continues to exhibit exponentially separating trajectory pairs for densities up to about 15% of the liquid density for the case of neon. Indeed although three-body and four-body collisions become significant at the higher densities, we show that a theoretical expression for the trajectory exponentiation rate, crudely derived for a hard-sphere gas, actually fits the Lennard-Jones data rather nicely over the density range studied. In short, the Lennard-Jones gas appears to exhibit the same type unstable $C$-system behavior[3] as does the hard-sphere gas,[7] at least for the densities considered here. Clearly, our computer calculations do not rule out the existence of regions of KAM stability, although we found none; obviously we can say nothing as yet about the system behavior as the liquid density is more closely approached. Our conclusions are thus quite tentative and we

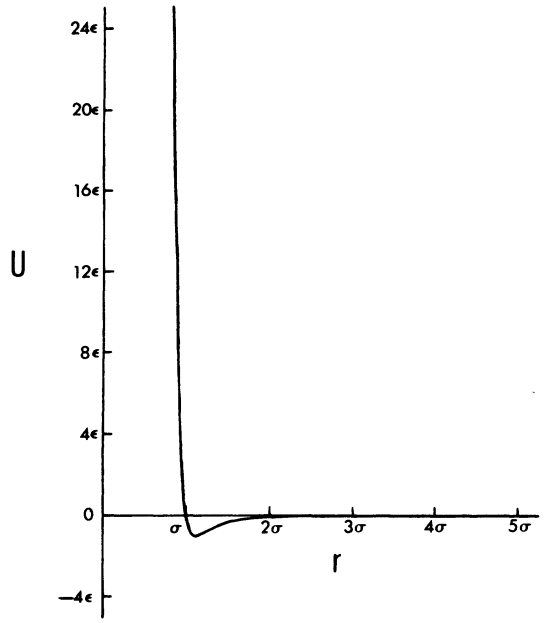


FIG. 1. Graph of the cut off Lennard-Jones interpartical potential $U$ as a function of interparticle distance $r$. Here $\sigma$ and $\epsilon$ are the standard Lennard-Jones parameters.

present them as only a crude signpost to guide subsequent investigators capable of greater mathematical rigor than ourselves.

## II. DISCUSSION OF THE LENNARD-JONES MODEL AND INTRODUCTION TO THE EXPERIMENTAL PROCEDURES

The Lennard-Jones pair potential $V(r)$ may be written in the standard form

$$V(r)=4\epsilon[(\sigma/r)^{12}-(\sigma/r)^{6}], \tag{1}$$

where $r$ denotes interparticle distance and where $\epsilon>0$ and $\sigma>0$ denote tabulated[8] Lennard-Jones parameters having the units of energy and distance, respectively. For convenience in the computer calculations, we modified the potential of Eq. (1) slightly by introducing a cutoff radius $r_c$ outside of which we set $V\equiv 0$. In particular we used the cutoff Lennard-Jones potential $U(r)$ given by

$$\begin{aligned}U(r)=4\epsilon\{&[(\sigma/r)^{12}-(\sigma/r)^{6}]\\&+[6(\sigma/r_c)^{12}-3(\sigma/r_c)^{6}](r/r_c)^{2}\\&-7(\sigma/r_c)^{12}+4(\sigma/r_c)^{6}\}\end{aligned} \tag{2}$$

for $r\leq r_c$, and $U(r)\equiv 0$ for $r\geq r_c$. Clearly Eq. (2) and Eq. (1) differ only slightly provided $r_c$ is taken several times the size of $\sigma$. In our numerical experiments, we set $r_c=5\sigma$; the potential of Eq. (2) is plotted in Fig. 1. The virtue of Eq. (2) for calculative purposes is that both $U$ and $dU/dr$ go continuously to zero as $r$ approaches $r_c$ from below; thus there are no discontinuous forces to contend with and any particle outside the $r_c$ range of all others moves as a free particle. To further ease the computer calculation, we expressed distance in units of $\sigma$, energy in units of $4\epsilon$, and mass in units of the single-particle mass; in these units, Eq. (2) may be written

$$\begin{aligned}U(r)=&[(1/r^{12})-(1/r^{6})]+[(6/r_c{}^{12})-(3/r_c{}^{6})](r/r_c)^{2}\\&-(7/r_c{}^{12})+(4/r_c{}^{6}).\end{aligned} \tag{3}$$

For comparison with a real gas, we list in Table I the relationship between our computer units and the mks units for neon; here m.u., l.u., t.u., and e.u. stand for computer units of mass, length, time, and energy, respectively. Finally then the Hamiltonian for our model system may be written

$$H=\tfrac{1}{2}\sum_i p_i{}^{2}+\sum_{i>j}U(r_{ij}), \tag{4}$$

where $p_i$ is the magnitude of the vector momentum of particle $i$, $U$ is given by Eq. (3), and $r_{ij}$ is the scalar magnitude of the distance between particles labeled $i$ and $j$.

Since we are here interested in demonstrating that Hamiltonian (4) has at least certain characteristics of a $C$ system, which latter is known to be ergodic and mixing, we briefly discuss those properties of $C$ systems germane to our calculations; for precise mathematical definitions, the

TABLE I. Conversion between computer and mks units for neon.

| Quantity | Computer units | mks units |
|---|---|---|
| Mass | 1 m.u. | $3.34\times10^{-26}$ kg |
| Length | 1 l.u. | $2.74\times10^{-10}$ m |
| Time | 1 t.u. | $1.12\times10^{-12}$ sec |
| Energy | 1 e.u. | $2.00\times10^{-21}$ J |
| $k_B$ (Boltzmann constant) | 0.00690 $\frac{\text{e.u.}}{\text{°K particle}}$ | $1.38\times10^{-23}$ $\frac{\text{J}}{\text{°K particle}}$ |
| $m$ (particle mass) | 1 m. u. | $3.34\times10^{-26}$ kg |
| $\sigma$ | 1 l.u. | $2.74\times10^{-10}$ m |
| $\epsilon$ | 0.25 e.u. | $5.00\times10^{-22}$ J |

reader is referred to the text by Arnold and Avez.[3] Let us consider small elements of hyperarea on an energy surface for Hamiltonian (4) and consider the flow of these areas generated by Hamiltonian (4) in time. This system is said to be a $C$ system (at the given energy) provided that every small hyperarea can be divided into precisely two subspaces, called the dilating and contracting subspaces, such that any two points in the dilating space separate exponentially with time while any two points in the contracting space approach each other exponentially. Mathematically if $\delta y(t)$ is the instantaneous Cartesian phase-space distance between two points, we require that

$$\delta y(t) \geq ae^{\lambda t}\,\delta y(0), \quad t \geq 0 \tag{5a}$$

$$\delta y(t) \leq be^{-\lambda t}\,\delta y(0), \quad t \leq 0 \tag{5b}$$

for $\delta y(0)$ in the dilating space, and

$$\delta y(t) \leq be^{-\lambda t}\,\delta y(0), \quad t \geq 0 \tag{6a}$$

$$\delta y(t) \geq ae^{\lambda t}\,\delta y(0), \quad t \leq 0 \tag{6b}$$

for $\delta y(0)$ in the contracting space, where the constants $\lambda$, $a$, and $b$ must be independent of $t$ and $\delta y(0)$.

We further require that the dimension of each subspace be unity or greater and that the sum of their dimensions be one less than that of the energy surface itself. Since the two subspaces each are of measure zero on the energy surface, we note that the distance between two initially close, arbitrary points on the energy surface will almost always be dominated by Eq. (5a) for $t \to \infty$, and by Eq. (6b) for $t \to -\infty$. In our calculations, we forward-integrated Hamiltonian (4) for a host of initially close phase-space points and, rather than the full phase-space distance, we separately computed the dimensionally homogeneous distances

$$D_q(t) = \left\{\sum_i [r_i'(t) - r_i(t)]^2\right\}^{1/2}, \tag{7}$$

$$D_p(t) = \left\{\sum_i [p_i'(t) - p_i(t)]^2\right\}^{1/2}, \tag{8}$$

where we use a prime to distinguish one point from the other and where $r_i$ and $p_i$ denote the vector position and momentum of particle $i$. Obviously if $D_q$ and $D_p$ separately grow exponentially, then so does the full phase-space distance $D = (D_q^2 + D_p^2)^{1/2}$. In every case investigated, the dimensionally homogeneous distances $D_q$ and $D_p$ both exhibited an exponential growth indicative of $C$-system behavior. Clearly this result does not prove that Hamiltonian (4) is a $C$ system because, aside from the obvious fact that not all trajectory pairs were integrated and shown to satisfy Eqs. (5) and (6), the two subspaces were not isolated and the correctness of their dimensionality verified. Actually a computer could in principle be used to determine these subspaces and their properties as Froeschle[9] has recently demonstrated for certain area-preserving mappings; however, his procedures would require more computer time than was available to us.

In order to verify the exponential growth of the distances defined by Eqs. (7) and (8), we actually calculated $\log_{10} D_q$ and $\log_{10} D_p$ as a function of time. Aside from fluctuations explicable on dynamic grounds, as expected these two quantities on the average grew linearly with time and we fitted the data with straight lines using a least-squares method. The slopes $\lambda_q$ and $\lambda_p$ of these lines, given by

$$\lambda_q = d\langle \log_{10} D_q \rangle / dt, \quad \lambda_p = d\langle \log_{10} D_p \rangle / dt, \tag{9}$$

where the angular brackets indicate a least-squares-derived quantity, provide the average rate of exponential growth for $D_q$ and $D_p$. We evaluated $\lambda_q$ and $\lambda_p$ for a 100-particle Lennard-Jones gas whose particles moved in the same two-dimensional box having periodic boundary conditions. Confining the system particles to move in only two dimensions yields a tremendous saving in computer time without any expected loss in generality since the two-dimensional hard-sphere gas in ergodic and mixing.[3] Periodic boundary conditions remove the spuriously large jumps in $D_q$ and $D_p$ which occur when two or more particles simultaneously collide with each other and with a fixed, reflecting wall. Such jumps correspond to surface effects which dominate in the relatively small system we treat, and we may avoid this effect by using periodic boundary conditions.

A fourth-order, variable step size, Runga-Kutta method[10] was used in all numerical integrations of Hamiltonian (4). Accuracy was monitored by regularly checking for the constancy of the known constants of the motion which remained constant to within about one part in $10^8$ for all our runs. In addition, various highly accurate runs were time reversed and integrated backward, quite accurately recovering the initial $(r_i, p_i)$ state. Derived quantities such as $\lambda_q$ and $\lambda_p$ were computed for these highly accurate runs as well as for less accurate runs starting from the same initial states. We thereby determined that we could reliably compute the needed derived quantities without necessarily being able to very accurately recover the initial state.[11] A single run, in our terminology, consists of integrating Hamilton's equations of motion simultaneously for two distinct trajectories. The two representative system points in phase space were initially separated by only a very small

distance—on the order of $10^{-7}$ in the units of Eq. (3). The equations of motion were then integrated until this distance grew by several orders of magnitude. Two groups of such runs were made. For the first and by far the largest group, the density was varied at approximately constant temperature. For the much smaller second group, the temperature was varied at constant density.

With these preliminaries completed, we may now embed an overview of our results in a further discussion of computational detail.

### III. SUMMARY OF RESULTS

In order to determine with any degree of certainty that most trajectory pairs on an energy surface separate exponentially, one needs a reasonable sampling of that surface, and here the sampling must be repeated for a set of energy surfaces generated by varying the density or the temperature. On the other hand, an exhaustive sampling of these energy surfaces for a 100-particle system would be prohibitively time consuming even on a high speed computer. Thus for each energy surface, we selected several sets of random initial conditions using a table of random numbers. Runs were started from each set of these initial conditions and, occasionally during each run, the coordinates and momenta as they existed at that time for one of the trajectories in the pair were saved for subsequent use as initial conditions in later runs. In turn, runs started from the "saved" data were used to similarly produce new runs, and so on. In view of the fact that, starting from the random initial sets of data, each trajectory pair was observed to be freely "exponentiating" over the energy surface while "generating" new runs of exponentially separating trajectory pairs, and so on, we concluded that the totality of our data represents at least a reasonable sampling of each energy surface. Additionally, the integration error introduced at each step of

TABLE II. Quantitative results of the numerical experiments at approximately constant temperature.

| Run No. | $\rho$ | % liq. $\rho$ | $T$ (°K) | $\lambda_p$ | $\lambda_q$ | $\lambda$ | 2B | 3B | 4B | $W$ | $t_r$ | $\tau$ | $\gamma_{expt}$ |
|---|---|---|---|---|---|---|---|---|---|---|---|---|---|
| 1 | 0.1200 | 14.8 | 327 | 0.935 | 1.09 | 1.01 | 64 | 9 | 2 | 88 | 2.14 | 1.22 | 2.83 |
| 2 | 0.1000 | 12.3 | 312 | 0.857 | 0.882 | 0.870 | 148 | 19 | 2 | 192 | 6.20 | 1.62 | 3.23 |
| 3 | 0.0800 | 9.84 | 310 | 0.705 | 0.704 | 0.704 | 182 | 10 | 0 | 202 | 9.84 | 2.44 | 3.95 |
| 4 | 0.0800 | 9.84 | 303 | 0.666 | 0.685 | 0.676 | 178 | 17 | 1 | 215 | 9.56 | 2.22 | 3.46 |
| 5 | 0.0600 | 7.38 | 300 | 0.690 | 0.705 | 0.697 | 91 | 5 | 0 | 101 | 6.15 | 3.05 | 4.89 |
| 6 | 0.0600 | 7.38 | 300 | 0.646 | 0.675 | 0.660 | 130 | 7 | 0 | 144 | 8.70 | 3.02 | 4.59 |
| 7 | 0.0600 | 7.38 | 305 | 0.791 | 0.830 | 0.810 | 123 | 7 | 1 | 140 | 7.15 | 2.55 | 4.76 |
| 8 | 0.0400 | 4.92 | 297 | 0.501 | 0.522 | 0.511 | 136 | 7 | 0 | 150 | 14.0 | 4.67 | 5.49 |
| 9 | 0.0400 | 4.92 | 290 | 0.504 | 0.507 | 0.505 | 129 | 5 | 0 | 139 | 13.9 | 5.00 | 5.82 |
| 10 | 0.0200 | 2.46 | 294 | 0.353 | 0.358 | 0.355 | 76 | 2 | 0 | 80 | 18.6 | 11.6 | 9.51 |
| 11 | 0.0200 | 2.46 | 295 | 0.557 | 0.559 | 0.558 | 64 | 2 | 0 | 68 | 13.9 | 10.2 | 13.1 |
| 12 | 0.0100 | 1.23 | 290 | 0.252 | 0.257 | 0.255 | 40 | 0 | 0 | 40 | 16.0 | 20.0 | 11.7 |
| 13 | 0.0080 | 0.984 | 290 | 0.203 | 0.206 | 0.205 | 62 | 0 | 0 | 62 | 33.8 | 27.3 | 12.8 |
| 14 | 0.0080 | 0.984 | 290 | 0.200 | 0.200 | 0.200 | 72 | 0 | 0 | 72 | 35.2 | 24.4 | 11.3 |
| 15 | 0.0060 | 0.738 | 290 | 0.177 | 0.183 | 0.180 | 50 | 1 | 0 | 52 | 36.2 | 34.8 | 14.4 |
| 16 | 0.0060 | 0.738 | 290 | 0.232 | 0.232 | 0.232 | 52 | 0 | 1 | 55 | 32.4 | 29.5 | 15.7 |
| 17 | 0.0040 | 0.492 | 290 | 0.157 | 0.162 | 0.159 | 48 | 0 | 1 | 51 | 43.5 | 42.7 | 15.6 |
| 18 | 0.0040 | 0.492 | 290 | 0.112 | 0.119 | 0.116 | 49 | 0 | 0 | 49 | 56.4 | 57.6 | 15.3 |
| 19 | 0.0040 | 0.492 | 289 | 0.146 | 0.157 | 0.152 | 42 | 0 | 0 | 42 | 44.7 | 53.2 | 18.6 |
| 20 | 0.0020 | 0.246 | 290 | 0.102 | 0.102 | 0.102 | 36 | 0 | 0 | 36 | 68.0 | 94.4 | 22.1 |
| 21 | 0.0010 | 0.123 | 290 | 0.052 | 0.054 | 0.053 | 28 | 0 | 0 | 28 | 100 | 179 | 21.9 |
| 22 | 0.0008 | 0.098 | 290 | 0.056 | 0.065 | 0.060 | 23 | 0 | 0 | 23 | 98.0 | 213 | 29.4 |
| 23 | 0.0008 | 0.098 | 290 | 0.080 | 0.087 | 0.084 | 16 | 0 | 0 | 16 | 69.0 | 216 | 41.5 |
| 24 | 0.0008 | 0.098 | 290 | 0.051 | 0.056 | 0.053 | 23 | 0 | 0 | 23 | 112 | 245 | 29.9 |
| 25 | 0.0004 | 0.049 | 290 | 0.040 | 0.042 | 0.041 | 12 | 0 | 0 | 12 | 100 | 418 | 39.1 |
| 26 | 0.0004 | 0.049 | 290 | 0.038 | 0.046 | 0.042 | 12 | 0 | 0 | 12 | 100 | 418 | 40.0 |
| 27 | 0.0004 | 0.049 | 290 | 0.018 | 0.022 | 0.020 | 14 | 0 | 0 | 14 | 172 | 616 | 28.2 |
| 28 | 0.0002 | 0.025 | 290 | 0.055 | 0.059 | 0.057 | 10 | 0 | 0 | 10 | 99.6 | 498 | 65.2 |
| 29 | 0.0002 | 0.025 | 290 | 0.025 | 0.027 | 0.026 | 19 | 0 | 0 | 19 | 214 | 562 | 33.8 |
| 30 | 0.0001 | 0.012 | 290 | 0.025 | 0.030 | 0.027 | 4 | 0 | 0 | 4 | 99.7 | 1247 | 78.7 |
| 31 | 0.0001 | 0.012 | 290 | 0.014 | 0.015 | 0.014 | 5 | 0 | 0 | 5 | 315 | 3150 | 104 |
| 32 | 0.0001 | 0.012 | 290 | 0.019 | 0.020 | 0.019 | 13 | 0 | 0 | 13 | 269 | 1036 | 46.2 |

the integration process itself subsequently increases exponentially, increasing the randomness of the total set of initial data over each energy surface.

Turning now to the runs themselves, all runs were processed in the same way whether the source of initial conditions was random numbers or a previous run. A given set of initial conditions were taken to be the unprimed variables of Eqs. (7) and (8). The given particle coordinates were then uniformly scaled to reach the desired system density, and any particles closer together than $(0.9)\sigma$ were separated to this distance. The total linear momentum was reduced to zero by subtracting $(1/N)$ times the total system momentum from the momentum of each particle, where $N$ is the number of particles in the system. The angular velocity of the system was found by applying the inverse of the inertia tensor to the total angular momentum, and the angular momentum was then reduced to zero by adding the negative of this angular velocity to the system as a whole. Last, the linear momenta were uniformly scaled to attain the desired total system energy (temperature). At this point if the initial conditions were derived from random numbers, the system was integrated until an approximately Maxwellian velocity distribution was obtained, ensuring that the subsequently computed $\lambda_q$ and $\lambda_p$ were characteristic of thermodynamics equilibrium states. Finally, the initial conditions for the primed variables in Eqs. (7) and (8) were obtained by making small displacements in the unprimed system variables of about $10^{-8}$ per particle in units of Eq. (3). Although, as mentioned earlier, the error in $D_q$ and $D_p$ itself grows exponentially, we could nonetheless detect the exponential growth of $D_q$ and $D_p$ by choosing their initial values to be significantly larger than the initial error.[12]

Typical experimental results obtained by varying the density at approximately constant temperature for an isolated, 100-particle system are presented in Table II. A number of distinct runs having the same density and temperature are presented in order to reveal the typical fluctuations of $\lambda$ which were observed in our calculations. With the exception of the temperature, all tabulated quantities are specified in computer units. The data for each run appears as a row in Table II and the first column lists for easy reference the number of the run. The second column lists the number density $\rho$ of particles per unit area. For comparison with a real gas, the third column of Table II lists the fraction $(\rho/\rho_L)$ in percentage, where $\rho_L$ is the liquid density of neon. The fourth column tabulates the system temperature $T$ in degrees Kelvin. Here $T$ represents the time average of the instantaneous kinetic temperature defined by

$$T=(Nk_B)^{-1}\sum_{i=1}^{N}(\tfrac{1}{2}mv_i^2), \tag{10}$$

where $N$ is total particle number, $k_B$ is the Boltzmann constant, $m$ is the particle mass, and $v_i$ is the speed of particle $i$. Because our system is isolated, the total system energy remains constant while the temperature fluctuates[13]; nonetheless, the instantaneous temperature fluctuations for our system were observed to be essentially negligible. The time-average temperature for each run in Table II is approximately the same.

The next two columns list the experimentally observed values of $\lambda_q$ and $\lambda_p$. As mentioned earlier, these numbers are the slopes of the straight lines resulting from a least-squares fit of the $\log_{10}D_q$ and $\log_{10}D_p$ versus time data. In Figs. 2–4, we show some typical examples of $\log_{10}D_q$ and $\log_{10}D_p$ plotted versus time. In these figures, $\log_{10}D_p$ and its fitted line are solid curves while $\log_{10}D_q$ and its line are the broken curves. In every case examined, we found an average linear growth of $\log_{10}D_q$ and $\log_{10}D_p$, indicating $C$-system behavior. As expected both $\lambda_q$ and $\lambda_p$ increase with increasing system density. Moreover, as might be anticipated on intuitive grounds, since at any instant the growth of $D_q$ depends on the change in $D_p$ during the previous collision and vice versa, we found $\lambda_q$ to always very nearly equal $\lambda_p$. Thus, in column seven, we list an overall average rate of exponential growth $\lambda$, where $\lambda$ is the arithmetic mean of $\lambda_q$ and $\lambda_p$; we henceforth drop the distinction between $\lambda_q$ and $\lambda_p$, always using the mean value $\lambda$.

The next four columns in the table, labeled 2B, 3B, 4B, and $W$, list the number of two-body, three-body, and four-body collisions followed by a

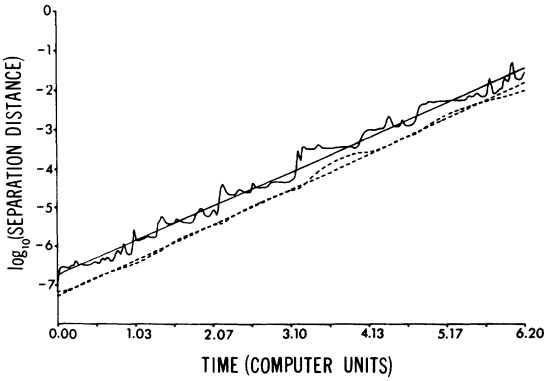


FIG. 2. Graph of $\log_{10}D_p$ and $\log_{10}D_q$, labeled $\log_{10}$ (separation distance), versus time for run 2 in Table II. Here and in the following two figures $\log_{10}D_p$ and its straight-line least-squares fit are solid curves while $\log_{10}D_q$ and its associated line are dashed curves.

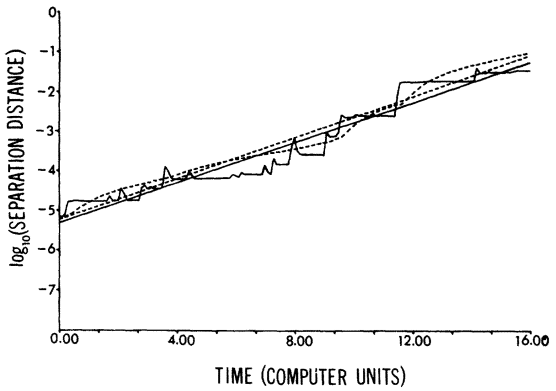


FIG. 3. Graph of $\log_{10}D_p$ and $\log_{10}D_q$, labeled $\log_{10}$ (separation distance), versus time for run 12 in Table II.

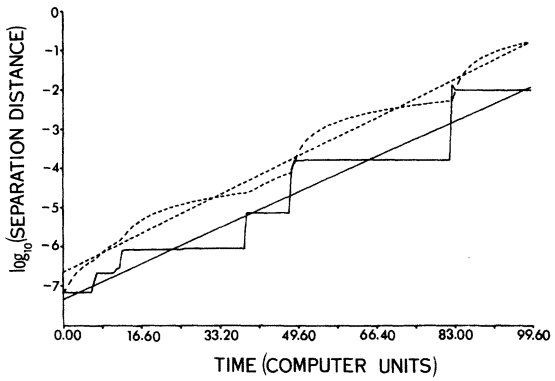


FIG. 4. Graph of $\log_{10}D_p$ and $\log_{10}D_q$, labeled $\log_{10}$ (separation distance), versus time for run 28 in Table II.

weighted sum $W$ of these collisions. No collisions simultaneously involving more than four particles were observed to occur. Here an $n$-body collision is defined as the formation and subsequent dissolution of a group of $n$ particles, where each member of the group was within a distance $\sigma$ [see Eq. (2)] of at least one other member of the group. A collision was counted when the first particle left the group, but not when successive particles did, unless a new particle joined the group before its complete dissolution. In this latter case, a new collision was counted when the first particle left the new group, and so on. In the weighted total $W$, three-body and four-body collisions were given the weights of two and three binary collisions. These weights represent the simplest sequences of binary collisions that would replace the multiple ones were this a hard-sphere gas, as we shall assume it to be in Sec. IV on theory, rather than a Lennard-Jones gas. Thus $W$ is the total number of "equivalent" binary collisions which occurred in each run.

The column following the collision data in Table II lists the time duration $t_\tau$ of each run. Expressing $t_\tau$ in real time units using Table I, one notes that our longest runs were of extremely short duration on a macroscopic scale—a few tenths of a nonosecond at most. Using $t_\tau$ and $W$, we can calculate the effective mean time $\tau$ between equivalent binary collisions for a single particle using

$$\tau = (Nt_\tau/2W) . \tag{11}$$

The value of $\tau$ for each run is listed in column 13 of Table II. In order to explain the last column in Table II, let us note that on the average both $D_q$ or $D_p$ grow exponentially according to the equation

$$D(t) = D(0)10^{\lambda t} . \tag{12}$$

Into Eq. (12) let us insert $t = n\tau$, where $n$ is the average number of equivalent binary collisions for a single particle which have occurred up to the time $t$. We then may write Eq. (12) as

$$D(n) = D(0)e^{\gamma n} , \tag{13}$$

where $\gamma = (\lambda\tau)\ln(10)$ is the average rate of exponential growth per single-particle equivalent binary collision. The last column in Table II, labeled $\gamma_{\text{expt}}$, tabulates the experimentally observed value of $\gamma$ which will be compared with a theoretically derived value of $\gamma$ in Sec. IV.

Finally, in Table III, we conclude the presentation of our experimental results by listing the data for a few runs made at constant density but different temperatures. We defer discussion of this table until Sec. IV.

## IV. COMPARISON OF EMPIRICAL RESULTS TO THEORETICAL CALCULATIONS FOR A HARD-SPHERE GAS

For a hard-sphere gas, the total system energy is purely kinetic; thus the system energy $E$ and

TABLE III. Quantitative results of the numerical experiments at constant density. The first line of this table is copied from Table II, run 12.

| $\rho$ | % liq. $\rho$ | $T$ (°K) | $\lambda_p$ | $\lambda_q$ | $\lambda$ | 2B | 3B | 4B | $W$ | $t_\tau$ | $\tau$ | $\gamma_{\text{expt}}$ |
|---|---|---|---|---|---|---|---|---|---|---|---|---|
| 0.0100 | 1.23 | 290 | 0.252 | 0.257 | 0.255 | 40 | 0 | 0 | 40 | 16.0 | 20.0 | 11.7 |
| 0.0100 | 1.23 | 435 | 0.420 | 0.440 | 0.430 | 40 | 0 | 0 | 40 | 10.1 | 12.6 | 12.5 |
| 0.0100 | 1.23 | 580 | 0.460 | 0.400 | 0.430 | 23 | 0 | 0 | 23 | 6.00 | 13.0 | 12.9 |
| 0.0100 | 1.23 | 725 | 0.410 | 0.430 | 0.420 | 40 | 0 | 0 | 40 | 11.3 | 14.1 | 13.7 |

the temperature $T$ are both constants of the motion with $E = Nk_B T$. Now consider two energy surfaces with the associated temperatures $T_1$ and $T_2$ ($T_2 > T_1$) and two trajectory pairs, with one pair on each surface. Suppose that initially the two trajectory pairs have the same configuration-space coordinates, $\{r_i\}$ for one trajectory of each pair and $\{r_i'\}$ for the other member of each pair; however, let the initial vector momenta $\{p_i\}$ and $\{p_i'\}$ of the trajectory pair on the lower energy surface be uniformly scaled up to $\{(T_2/T_1)^{1/2} p_i\}$ and $\{(T_2/T_1)^{1/2} p_i'\}$, yielding the initial momenta of the higher-energy trajectory pair. Here the temperature is different for each trajectory pair but the particle density is the same.

With these initial conditions, the two configuration-space trajectories for the lower-temperature pair are identical to those of the higher-temperature pair; in particular, the representative system points for the higher-temperature pair merely traverse the same configuration-space trajectories as the lower-temperature pair but at a more rapid rate. Consequently, using Eq. (13), we see that $D_q(0)$, $D_q(n)$, and $\gamma_q$ are identical for the two trajectory pairs; moreover, since $D_p(0)$ and $D_p(n)$ for the two energy surfaces differ only by the scale factor $(T_2/T_1)^{1/2}$, the momenta $\gamma_p$ are the same for the two trajectory pairs also. In addition, as we shall discuss shortly, $\gamma_q = \gamma_p$ and we drop the subscript on $\gamma$. Finally then, for the hard-sphere gas, we conclude that $\gamma$ is independent of temperature for fixed density, although $\gamma$ may vary over a specified energy surface. Now examining Table III, we note that $\gamma$ for our Lennard-Jones system is also rather insensitive to varying the temperature while holding the density constant, indicating that the Lennard-Jones gas here behaves much like the hard-sphere gas. In Table III, the initial conditions of the trajectory pairs on the various energy surfaces were not "scaled" as discussed above; the computer values of $\gamma$ are nonetheless approximately constant, indicating that $\gamma$ may depend less sensitively than $\lambda$ on energy-surface position.

Emboldened by this success in relating hard-sphere-gas behavior to that of the Lennard-Jones gas at least over the density range considered, we then derived an analytic expression for $\gamma$ using hard-sphere-gas dynamics. This derivation, which is tediously long and which includes many plausibility arguments, is presented in detail elsewhere.[14] Here we shall only write down the final expression for $\gamma$ and justify it only in terms of plausibility arguments. Finally, we shall compare this hard-sphere-gas expression for $\gamma$ with the $\gamma_{\text{expt}}$ of Table I.

The derived expression for $\gamma$ is

$$\gamma = \beta\{\cosh^{-1}[1 + (\pi^{3/2} u\tau / 2^{1/2}\beta d)] - \ln(4)\}, \quad (14)$$

where $u$ is the average single-particle speed, $\tau$ is the mean time between binary collisions, $d$ is the hard-sphere diameter, and $\beta$ is a parameter depending only on total system particle number $N$. In Eq. (14), the dependence of $\gamma$ on the product $u\tau$, which equals the mean free path between binary collisions, is quite reasonable. As the mean free path between collisions increases, the two system trajectories have increasing time to stream apart in configuration space causing a larger increase in $D_q$ per collision. Additionally, this increased streaming creates increasingly different "initial" collision parameters for each binary collision thereby increasing $D_p$ per collision. Lastly this mean-free-path dependence of $\gamma$ implies, in agreement with our previous argument, that $\gamma$ varies with density but not with temperature.

The explanation of the functional dependence $\gamma \sim (\cosh^{-1})$ in Eq. (14) is also relatively straightforward. Roughly speaking, the momentum separation distance and the position separation distance after $n+1$ binary collisions are each related by a linear, first-order difference equation to the same quantities after $n$ collisions. Indeed, these quantities were both found to satisfy independently the same linear, second-order difference equation which could be reduced to the form

$$A_{n+2} + 2CA_{n+1} + A_n = 0, \quad (15)$$

where the parameter $C$ is greater than unity. An equation of this type has the growing exponential solution $A_n \sim e^{\gamma n}$, where $\gamma = \cosh^{-1} C$; this then is the source of $(\cosh^{-1})$ in Eq. (14). Moreover, since both the momentum separation distance and the position separation distance satisfy the same difference equation, one has $\gamma_q = \gamma_p = \gamma$ in agreement with our empirical results. Finally the constant term (ln4) in Eq. (14) was introduced to transform the original second-order difference equation into Eq. (15).

The factor $\beta$ in Eq. (14) accounts for the somewhat unexpected type of collision sequences which were observed to dominate and determine $D_q(n)$ and $D_p(n)$. Initially we anticipated that the single-particle differences $\delta r_i$ or $\delta p_i$ in Eqs. (7) and (8) would each have the same exponential growth on the average and would each therefore contribute equally to the sums in $D_q$ or $D_p$. In short we anticipated that each $\delta r_i$ or $\delta p_i$ would grow exponentially owing to uncorrelated binary collisions. However, this was found not to be the case and, indeed, a rather unusual type of correlation between collisions was observed in the empirical data. After starting a calculation with the $\delta r_i$ and $\delta p_i$ approximately equal in magnitude, it was

empirically observed that very quickly (about ten binary collisions in the whole system) some one term ($\delta r_i$) in Eq. (7) and the corresponding term ($\delta p_i$) in Eq. (8) dominate the sums in these equations. These maximum $\delta r_i$ and $\delta p_i$ were then observed to propagate via binary collisions from particle to particle, growing exponentially with each collision. As a consequence, $D_q$ and $D_p$ actually depend not on the average number $n$ of binary collisions for a single particle, nor on the average mean time $\tau$ between collisions, but on the number $n^*$ of binary collisions in the maximum sequences and on the mean time $\tau^*$ between binary collisions in this dominant sequence. In order to express $D_q$ and $D_p$ in terms of the more easily measured quantities $n$ and $\tau$, we began with Eq. (13) written as

$$D(n^*) = D(0)e^{\gamma^* n^*} . \tag{16}$$

We then defined $\beta$ via $n^* = \beta n$, writing

$$D(n) = D(0)e^{\beta\gamma^* n} . \tag{17}$$

Comparing Eq. (17) and Eq. (13), we see that $\gamma = \beta\gamma^*$. In Eq. (14), the expression for $\gamma^*$ appears inside the curly bracket, while the exterior multiplicative factor $\beta$ merely reflects the change from $n^*$ to $n$. Using $t = n^*\tau^* = n\tau = \beta n\tau^*$, we see that $\tau^* = \tau/\beta$; consequently, in Eq. (14), the factor $(\tau/\beta)$ gives the "effective" mean time between collisions. Finally, using an extremely crude argument, [15] we estimated that $\beta = \ln N$.

Having presented these intuitive arguments supporting the general analytic form of $\gamma$, let us now compare this theoretical equation with experiment. In Fig. 5 we graph $\gamma$ vs $\tau$; here the dots are empirical points for the Lennard-Jones gas at constant temperature taken from Table II, while the solid line is a plot of Eq. (14). Except at large $\tau$, the agreement between theory and experiment is surprisingly good; however, the disagreement at large $\tau$ is easily explained. Here two initially close trajectories stream far apart in configuration space before very many binary collisions occur, as can be seen in Fig. 4, for example. In particular not enough binary collisions occur in the whole system to initiate a dominant collisions sequence as required for the validity of our theory. Consequently Fig. 5 provides relatively strong evidence for $C$-system behavior in the Lennard-Jones gas over the density range considered. Indeed, ignoring the theoretical derivation of Eq. (14) and regarding it only as an empirical formula derived by curve fitting, we note that an analytical curve which nicely fits the relatively low-density region corresponding to $\tau = 10$ to 100 also fits equally well the higher-density region corresponding to $\tau = 1$ to 10. Because of this smooth extrapolation from lower to higher density, we conclude that over the density range studied here most trajectory pairs for the Lennard-Jones gas indeed separate exponentially just as do those of a hard-sphere gas; in particular, regions of KAM stability, if they exist, appear to be of negligible size.

## V. SUMMARY

Although the hard-sphere gas is known to be ergodic and mixing, the extent to which this behavior persists for systems having attractive as well as repulsive forces is unclear. In this investigation we numerically integrated the equations of motion for a Lennard-Jones gas and showed that, over a fairly wide density range, this system mimics that essential hard-sphere-gas behavior which is required for proving ergodicity and mixing, namely, an exponential separation with time of most initially close phase-space trajectories. Certainly our studies cannot rule out stable, nonergodic phase-space regions; however, they do indicate that such regions, if they exist, are likely to be quite small at least over the density range studied. In terms of neon, our investigation covered the density range from very dilute, ideal-gas densities up to 15% of the liquid density. In more absolute terms, the low-density system exhibited only binary collisions while three-body and four-body collisions were frequent at the higher densities.

In addition to demonstrating that the Lennard-Jones gas possesses exponentially separating trajectories, we numerically determined the rate of exponential separation as a function of density. Using very crude arguments involving an empir-

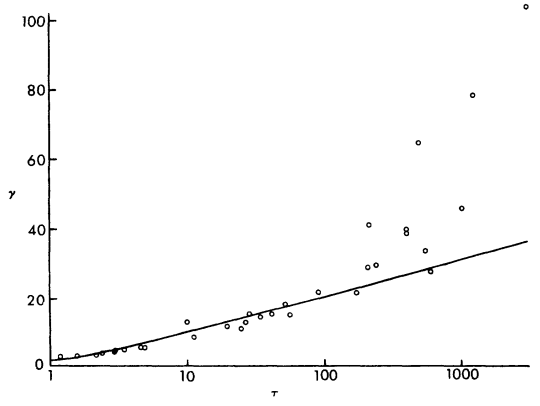


FIG. 5. Comparison of theoretical (solid curve) and experimental (small circles) values for the exponentiation rate per collision $\gamma$ as a function of mean time between binary collisions $\tau$.

ically observed dominant collision sequence, we calculated an expression for this exponentiation rate for a hard-sphere gas; the resulting theoretical curve fit the Lennard-Jones-gas data quite well over most of the density range investigated. Moreover, the exponentation rate of the Lennard-Jones gas was empirically observed to be quite insensitive to varying the temperature, another fact predicted using hard-sphere-gas dynamics. Thus the combined evidence presented here provides strong empirical support in favor of ergodicity and mixing for even a relatively dense Lennard-Jones gas.

ACKNOWLEDGMENT

The authors are indebted to Professor Richard H. Miller, Institute for Computer Research, University of Chicago, for supplying them with certain unpublished results concerning his work (Ref. 12) on the exponential separation of trajectories for small stellar dynamic systems.

---

*Research sponsored by the Air Force Office of Scientific Research under Grant No. AFOSR-73-2453.

[1]D. ter Haar, *Elements of Statistical Mechanics* (Rinehart, New York, 1954), Appendix I.

[2]Ja. G. Sinai, Russ. Math. Surv. **25**, 137 (1970).

[3]V. I. Arnold and A. Avez, *Ergodic Problems of Classical Mechanics* (Benjamin, New York, 1968), Chap. 3.

[4]A. S. Wightman, in *Statistical Mechanics at the Turn of the Decade*, edited by E. G. D. Cohen (Marcel Dekker, New York, 1971), p. 1.

[5]G. H. Walker and J. Ford, Phys. Rev. **188**, 416 (1969). Also consult Chap. 4 of Ref. 3.

[6]J. Ford, Adv. Chem. Phys. **24**, 155 (1973).

[7]D. V. Anosov and Ja. G. Sinai, Russ. Math. Surv. **22**, 103 (1967). Although strictly speaking the hard-sphere gas is not a *C* system, the two are intimately related, as is discussed on pp. 106–107 of this reference and on p. 78 of Ref. 3.

[8]C. Kittel, *Introduction to Solid State Physics* (Wiley, New York, 1966), pp. 81–85.

[9]C. Froeschle and J. Scheidecker, Astron. Astrophys. **22**, 431 (1973); J. Comput. Phys. **11**, 423 (1973).

[10]*Handbook of Mathematical Functions*, edited by M. Abramowitz and I. A. Stegun (U.S. Dept. of Commerce, National Bureau of Standards, Washington, D.C., 1964), p. 897.

[11]S. D. Stoddard, Ph.D. thesis (Georgia Institute of Technology, 1973) (unpublished), p. 81.

[12]R. H. Miller, Astrophys. J. **140**, 250 (1964).

[13]D. ter Haar, Ref. 1, p. 132.

[14]S. D. Stoddard, Ref. 11, Chap. 3.

[15]S. D. Stoddard, Ref. 11, p. 59.